1521-009X/12/4012-2315–2323$25.00
DRUG METABOLISM AND DISPOSITION
DMD 40:2315–2323, 2012

Vol. 40, No. 12
46821/3805047

Reversible Disulfide Formation of the Glutamate Carboxypeptidase II Inhibitor E2072 Results in Prolonged Systemic Exposures In Vivo

Rana Rais, Randall Hoover, Krystyna Wozniak, Michelle A. Rudek, Takashi Tsukamoto, Jesse Alt, Camilo Rojas, and Barbara S. Slusher

Brain Science Institute, NeuroTranslational Drug Discovery Program, (R.R., K.W., T.T., J.A., C.R., B.S.S.), Departments of Neurology (R.R., T.T., B.S.S.), Psychiatry (B.S.S.), and Oncology (M.A.R.), Johns Hopkins School of Medicine, Baltimore, Maryland; and Eisai, Inc., Baltimore, Maryland (R.H., K.W., T.T., J.A., C.R., B.S.S.)

Received May 21, 2012; accepted September 4, 2012

ABSTRACT:

E2072 [(3-2-mercaptoethyl)biphenyl-2,3′-dicarboxylic acid] is a novel, potent and selective thiol-based glutamate carboxypeptidase II (GCP-II) inhibitor that has shown robust analgesic and neuroprotective efficacy in preclinical models of neuropathic pain and chemotherapy-induced peripheral neuropathy. For the first time, we describe the drug metabolism and pharmacokinetic profile of E2072 in rodents and primates. Intravenously administered E2072 was found to exhibit an unexpectedly long terminal half-life (105 ± 40 h) in rats. The long half-life was found to be the result of its ability to rapidly form reversible homo- and possibly heterodisulfides that served as a continuous E2072 depot. The half-life of reversible homodisulfides was 208 ± 81 h. In further support, direct intravenous administration of the E2072-homodisulfide in rats resulted in the formation of E2072, with both E2072 and its disulfide detected in plasma up to 7 days after dose. The observed long exposures were consistent with the sustained efficacy of E2072 in rodent pain models for several days after dose cessation. It is noteworthy that a shorter $t_{1/2}$ of E2072 (23.0 ± 1.2 h) and its homodisulfide (21.0 ± 0.95 h) was observed in primates, indicating interspecies differences in its disposition. In addition, E2072 was found to be orally available with an absolute bioavailability of ~30% in rats and ~39% in monkeys. A tissue distribution study of E2072 and its homodisulfide in rats showed good tissue penetration, particularly in sciatic nerve, the presumed site of action for treatment of neuropathy. Metabolic stability and the correlation between pharmacokinetic profile and pharmacological efficacy support the use of this GCP-II inhibitor in the clinic.

Introduction

E2072 [(3-2-mercaptoethyl)biphenyl-2,3′-dicarboxylic acid] belongs to a family of thiol-based inhibitors of membrane-bound zinc metalloenzyme, glutamate carboxypeptidase-II (GCP-II; EC 3.4.17.21). GCP-II, also known as prostate-specific membrane antigen, *N*-acetylated α-linked acidic dipeptidase, and folate hydrolase, is a 94-kDa metalloenzyme that catalyzes the hydrolysis of neuropeptide *N*-acetyl-aspartyl glutamate (NAAG) to *N*-acetyl-aspartate and glutamate (Slusher et al., 1990; Neale et al., 2005, 2011). Glutamate is a major excitatory neurotransmitter in the central and peripheral nervous systems. Excessive concentrations of extracellular glutamate, possibly derived from NAAG hydrolysis, has been implicated in numerous neurological disorders, such as stroke, spinal cord injury, amyotrophic lateral sclerosis, peripheral neuropathy, chronic pain, dementia, Parkinson's disease, and cognition (Neale et al., 2011; Bařinka et al., 2012). Inhibition of GCP-II is thought to be a viable strategy for attenuation of glutamatergic effects both by causing an increase in NAAG and simultaneously decreasing the glutamate level (Bařinka et al., 2012; Rahn et al., 2012; Wozniak et al., 2012). 2-PMPA [2-(phosphonomethyl pentanedioic acid)] (Jackson et al., 2001) was the first highly potent and selective GCP-II inhibitor that displayed efficacy in preclinical models, including protection against ischemic injury (Slusher et al., 1999), cocaine addiction (Xi et al., 2010a,b), neuropathic pain and peripheral neuropathies (Yamamoto et al., 2001a; Chen et al., 2002; Marmiroli et al., 2012; Wozniak et al., 2012), formalin-induced agitation behavior (Yamamoto et al., 2001b), and seizures (Witkin et al., 2002; Luszczki et al., 2006), thus emphasizing its relevance as a therapeutic target, especially for the treatment of neurodegenerative diseases where excess glutamate is presumed pathogenic.

One of the biggest hurdles in design of a successful GCP-II inhibitor has been attainment of optimal physicochemical and biopharmaceutical properties. Early efforts led to the identification of extremely potent GCP-II inhibitors containing phosphonate (e.g., 2-PMPA, IC_{50} = 300 pM) and phosphinate functional groups that were potent in vitro (Slusher et al., 1999; Harada et al., 2000; Jackson et al., 2001; Tsukamoto et al., 2002). The downside of these functionalities was the extremely hydrophilic nature of the molecules, which impeded their permeation across blood-brain barrier, and consequently led to poor in

This work was supported in part by the National Institutes of Health National Cancer Institute [Grant R01-CA161056] (to B.S.S.).

Article, publication date, and citation information can be found at http://dmd.aspetjournals.org.

http://dx.doi.org/10.1124/dmd.112.046821.

ABBREVIATIONS: E2072, (3-2-mercaptoethyl)biphenyl-2,3′-dicarboxylic acid; GCP-II, glutamate carboxypeptidase-II; NAAG, *N*-acetyl-aspartyl glutamate; 2-MPPA (GPI 5693), 2-(3-mercaptopropyl)pentanedioic acid; 2-PMPA, 2-(phosphonomethyl pentanedioic acid); HPLC, high-performance liquid chromatography; NEM, *N*-ethylmaleimide; TCEP, tris-carboxyethyl phosphine; LC-MS/MS, liquid chromatography/tandem mass spectrometry; MRM, multiple reaction monitoring.

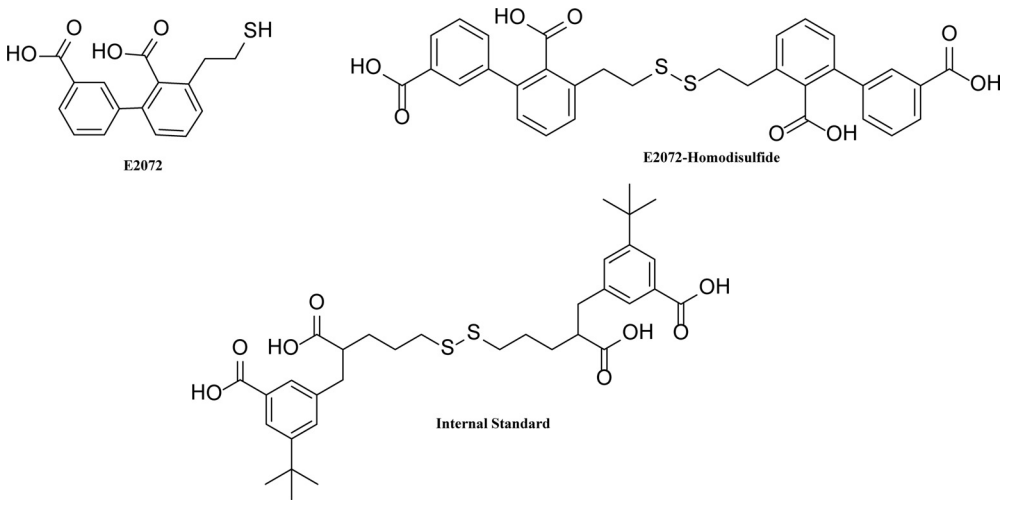

FIG. 1. Chemical structures of E2072, E2072-homodisulfide, and the internal standard.

vivo potency. Replacement of the phosphonomethyl group with the thioalkyl groups, with the assumption that this could result in significant improvement in oral bioavailability, led to the discovery of 2-MPPA [2-(3-mercaptopropyl)pentanedioic acid], also known as GPI 5693. 2-MPPA, which exhibited nanomolar level potency (IC_{50} = 90 nM) and efficacy in several animal models of disease after oral administration (Ghadge et al., 2003; Majer et al., 2003), was the first GCP II inhibitor to advance to the clinic where doses up to 1 g were found to be safe and well tolerated in healthy and diabetic subjects after acute and 14-day administration (van der Post et al., 2005). However, the concerns over potential immune reactivity common to thiol-containing drugs when dosed at high levels halted 2-MPPA clinical development. Because immune reactivity is often considered a function of dose, more potent compounds in this class were then sought.

Here, we report on the pharmacokinetics and metabolism of a promising, second generation thiol-based GCP-II inhibitor, E2072. E2072 is a highly selective and potent compound with approximately 10- to 100-fold more potent in vitro enzyme inhibition relative to 2-MPPA (K_i = 1–10 vs. 90 nM, respectively) and 10- to 100-fold more potent efficacy in in vivo preclinical neuropathy models (minimally effective dose of 0.1 vs. 10 mg/kg) (Carozzi et al., 2010; Stoermer et al., 2012). Oral administration of E2072 in rat models of peripheral neuropathy was found to relieve neuropathic pain symptoms while simultaneously slowing nerve conduction velocity decline (Carozzi et al., 2010). Furthermore, results indicated that GCP-II inhibition protects against the pathological changes of diabetes-induced axonal atrophy and Wallerian degeneration (Zhang et al., 2002, 2006). E2072 contains a terminal thiol functional group. Terminal thiols, such as in captopril, have been shown to be reactive both in vivo and in vitro (Drummer and Jarrott, 1984; Drummer et al., 1985), with the potential to form disulfide dimers and mixed disulfides with other free thiols upon entering the systemic circulation. Bearing this in mind, the studies presented here were aimed at delineating not only the pharmacokinetics of the parent drug E2072 but also the pharmacokinetics of its homodisulfide, which in preliminary studies was identified in high concentrations in plasma on administration of E2072.

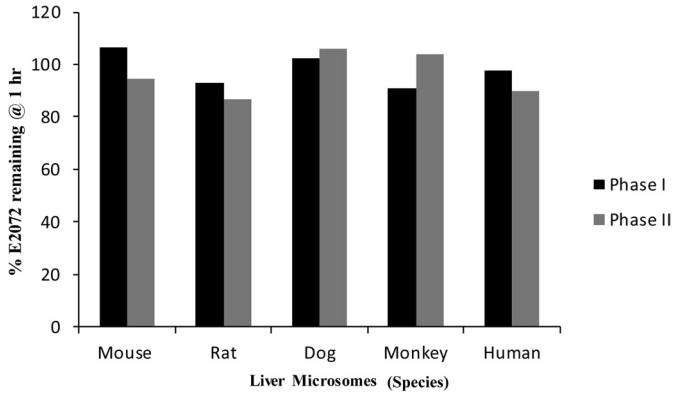

FIG. 2. Phase I and phase II metabolic stability of E2072 in liver microsomes from mouse, rat, dog, monkey, and human. Experiments were performed in duplicate, and the percentage remaining at 1 h is reported.

Materials and Methods

Chemicals and Reagents. E2072 and its homodisulfide were synthesized at Eisai, Inc. (Andover, MA). Drug-free rat and monkey heparin plasma, rat whole blood, and monkey and rat sera were obtained from Innovative Research, Inc. (Plymouth, MN). Liver microsomes from mouse, rat, dog, monkey, and humans, the NADPH-regenerating system, and UGT reaction mixture were purchased from BD Biosciences (San Jose, CA). Formic acid (98%, v/v in water) acetonitrile (HPLC grade) and methanol (HPLC grade) were obtained from EMD Chemicals, Inc. (Gibbstown, NJ). All of the chemical reagents were purchased from Sigma-Aldrich (St. Louis, MO) except where indicated. All solvents used were of HPLC grade.

In Vitro Metabolic Stability. Phase I and phase II metabolic stability of E2072 was conducted in liver microsomes from different species (i.e., mouse, rat, dog, monkey, and human). For phase I metabolism, the reaction was carried out with 100 mM potassium phosphate buffer, pH 7.4, in the presence of NADPH-regenerating system (1.3 mM NADPH, 3.3 mM glucose 6-phosphate, 3.3 mM $MgCl_2$, 0.4 U/ml glucose-6-phosphate dehydrogenase, 50 μM sodium citrate). Reactions in duplicate were initiated by addition of the appropriate liver microsomes to the incubation mixture (compound final concentration was 10 μM; 0.5 mg/ml microsomes). For phase II glucuronidation reaction, E2072 was added to Tris-HCl buffer (50 mM, pH 7.5) with microsomes (0.5 mg/ml), along with $MgCl_2$ (8 mM) and alamethicin (25 μg/ml) and preincubated at 37°C. The reaction was initiated (in duplicate) with uridine 5'-diphospho-glucuronic acid (2 mM; final concentration). Controls in the absence cofactors were carried out to determine the specific cofactor-free degradation. At predetermined times up to 1 h, aliquots of the mixture were removed, and the reaction was quenched by addition of two times the volume of ice-cold acetonitrile spiked with the internal standard. Compound disappearance was monitored over time using a liquid chromatography and tandem mass spectrometry (LC-MS/MS) method.

In Vitro Blood to Plasma Ratio, Plasma Stability, and Serum Protein Binding. Blood to plasma ratio was determined as described previously (Fukuda et al., 2008; Akabane et al., 2009; Bungay et al., 2011; Jayaraman et

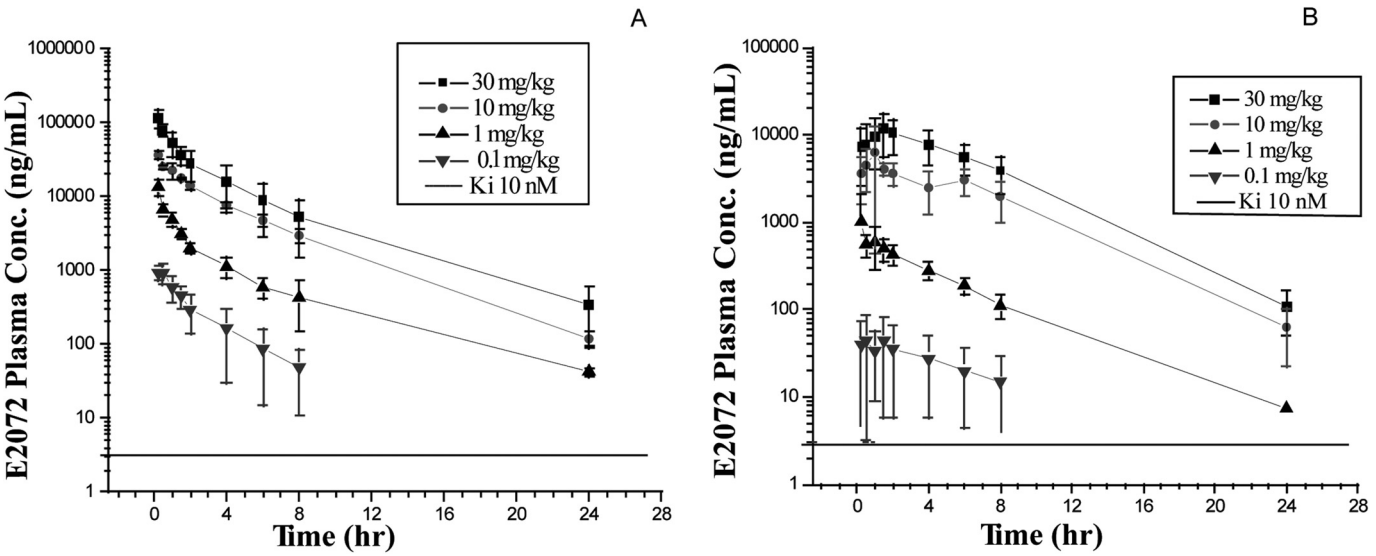

FIG. 3. Concentration-time profiles following intravenous administration (A) and oral administration (B) of E2072 in male Sprague-Dawley rats under fasted conditions.

al., 2011) with minor modifications. In brief, fresh blood from male Sprague-Dawley rats was spiked with E2072 at a concentration of 10 μM and incubated at 37°C for 10 min; a preliminary study confirmed that 10 min was sufficient to reach equilibrium. Blood sample aliquots were withdrawn, and the remaining sample was centrifuged at 4000 rpm (1800*g*) for 10 min to obtain plasma. The blood and plasma samples were extracted with acetonitrile-methanol (7:3, v/v), vortexed, and centrifuged. The resultant supernatants were analyzed by LC-MS/MS. The blood to plasma ratio was calculated as C_b/C_p, where C_b and C_p represent the blood and plasma concentrations of the compound, respectively.

For plasma stability, compound (5 and 10 μM) was spiked in plasma from Sprague-Dawley rats and cynomolgus monkeys and incubated at 37°C. At 0, 30, and 60 min, 150-μl aliquots were withdrawn, and the reaction stopped at by addition of 300 μl of acetonitrile. Samples were vortexed and centrifuged, and the resultant supernatants were analyzed by LC-MS/MS. The percentage remaining was calculated as A_t/A_o, where A_o was the area ratio (ratio of area of analyte to internal standard) at time 0 and A_t was the area ratio at the specified time of incubation.

For protein binding, sera from Sprague-Dawley rats and cynomolgus monkeys were spiked with E2072 (10 μM) and incubated at 37°C for 1 h. A 500-μl aliquot was then added to the sample reservoir portion of the ultrafiltration device (Corning Spin-X UF with a molecular mass cutoff of 5000 Da) and centrifuged for 45 min at 37°C and 4000 rpm (1800*g*). The concentrations were determined in both the filtrate and serum before filtration after extraction and quantified via LC-MS/MS. Protein binding was calculated as percentage bound = $100 - [(C_u/C_s) \times 100]$, where C_u was the concentration in the ultrafiltrate and C_s was the concentration in the serum.

E2072 Pharmacokinetics in Rats. All of the animal studies were performed as per protocols approved by the Institutional Animal Care and Use Committee.

E2072 was administered to male Sprague-Dawley rats (weighing 280–330 g) as a single oral or intravenous dose. Rats were fasted overnight until 4 h after dose. Dosing solutions were prepared in 50 mM HEPES buffered saline, pH 7.4. Rats were jugular vein cannulated and received a 0.1, 1, 10, and 30 mg/kg concentration of the dosing solution by oral gavage (*n* [mteq] 4) or 0.1, 1, 10, and 30 mg/kg i.v. (*n* [mteq] 7), administered as a bolus injection in the tail vein. To assess the effect of food in male Sprague-Dawley rats, E2072 dosing solution was prepared in 50 mM HEPES buffered saline, pH 7.4, and administered to rats as a single oral dose of 10 mg/kg under nonfasted conditions. Blood samples were collected in heparinized microtubes containing 10 μl of 100 mM *N*-ethylmaleimide (NEM) at 0, 0.25, 0.5, 1, 2, 4, 6, 8, and 24 h after dosing. Plasma was prepared by centrifugation immediately after collection of blood samples. All plasma samples were stored at or below −20°C until analyzed for E2072 by LC-MS/MS method as described in the bioanalytical section.

E2072-Homodisulfide Pharmacokinetics in Rats. Male Sprague-Dawley rats were dosed intravenously with E2072 at 10 mg/kg ($n = 6$) or its homodisulfide at 5 mg/kg ($n = 5$) in a similar manner as described above. To fully characterize the terminal elimination, blood sample collection was extended up to 7 days after dose in heparinized microtubes containing 10 μl of 100 mM NEM. The plasma obtained from blood was analyzed for E2072 and E2072-homodisulfide. To examine whether the observed dimer was a contaminant from the dosing solution or a metabolite of E2072, dimer-free E2072 dosing solution (10 mg/kg) was prepared by using a thiol-reducing agent, tris-carboxyethyl phosphine (TCEP) solution, at 1.5 mg/ml. The TCEP-treated dose solution was administered to rats either intravenously or orally. The absence of E2072-homodisulfide in the dosing solutions was verified by LC-MS/MS.

E2072 and E2072-Homodisulfide Pharmacokinetics in Monkeys. E2072 was administered by intravenous bolus and orally to cynomolgus monkeys ($n = 3$) at a nominal dose of 5 mg/kg. The dosing solutions (in 50 mM HEPES)

TABLE 1

E2072 plasma pharmacokinetic parameters in rats[a]

	C_{max}	T_{max}	AUC_{last}	AUC_{inf}	Cl[b]	V_d[b]	$t_{1/2}$	%F
	ng/ml	*h*	*ng · h/ml*		*l/h/kg*		*h*	
0.1 mg/kg i.v.			1800 ± 927	1969 ± 1071	0.06 ± 0.03	0.20 ± 79	2.30 ± 0.23	
0.1 mg/kg p.o.	62.6 ± 43.0	0.83 ± 0.77	268 ± 267	605 ± 939	0.51 ± 0.40	2.98 ± 1.45	9.33 ± 14.9	17.4 ± 17.3
1 mg/kg i.v.			12,675 ± 7417	12,989 ± 7511	0.05 ± 0.03	0.21 ± 0.11	3.25 ± 1.13	
1 mg/kg p.o.	1095 ± 1058	0.58 ± 0.44	2608 ± 818	3209 ± 776	0.33 ± 0.09	1.65 ± 0.69	3.72 ± 2.25	23.7 ± 6.6
10 mg/kg i.v.			90,150 ± 88,864	90,622 ± 9043	0.27 ± 0.12	1.43 ± 0.82	3.55 ± 0.61	
10 mg/kg p.o.	7097 ± 5549	1.03 ± 0.57	33,448 ± 9737	33,762 ± 9867	0.32 ± 0.09	1.44 ± 0.46	3.17 ± 0.60	37.3 ± 10.9
30 mg/kg i.v.			202,098 ± 86,045	204,159 ± 86,969	0.18 ± 0.08	1.08 ± 0.78	4.07 ± 0.98	
30 mg/kg p.o.	13,017 ± 6148	1.43 ± 0.35	76,062 ± 26,257	76,570 ± 26,341	0.51 ± 0.40	2.39 ± 2.18	3.15 ± 0.46	37.5 ± 12.9

[a] Data are presented as mean ± S.D.; $n = 4$–9 rats per dose group.
[b] For intravenous data, Cl and V_d are presented. For oral data, apparent clearance (Cl/*F*) and apparent volume (V_d/F) are presented.

TABLE 2

Plasma pharmacokinetic parameters in rats following 10 mg/kg p.o. E2072 under fasted and fed conditions[a]

	C_{max}	T_{max}	AUC_{last}	AUC_{inf}	Cl[b]	V_d[b]	$t_{½}$
	ng/ml	*h*	*ng · h/ml*		*l/h/kg*	*l/kg*	*h*
E2072 Fasted	7097 ± 5549	1.03 ± 0.57	33,448 ± 9737	33,762 ± 9867	0.32 ± 0.09	1.44 ± 0.46	3.17 ± 0.60
E2072 Fed	16,186 ± 15,426	0.29 ± 0.1	32,213 ± 10,057	37,057 ± 12,942	0.30 ± 0.09	1.09 ± 0.22	2.75 ± 0.97

[a] Data are presented as mean ± S.D.; n = 6–9 rats per dose group.
[b] For oral data, apparent clearance (Cl/F) and apparent volume (V_d/F) are presented.

were treated with TCEP to prevent the formation of homodisulfide in dosing solution. The intravenous dose was administered via either the cephalic or saphenous vein, and blood collection was via cannulas implanted in either the iliac or femoral artery. Blood samples were taken up to 9 days after dose in heparinized microtubes containing 10 μl of 100 mM NEM. Plasma from the blood samples was analyzed for E2072 and its homodisulfide dimer (E2072-homodisulfide) by LC-MS/MS.

Tissue Distribution after Single and Multiple Daily Oral Dosing. Tissue distribution study in male Sprague-Dawley rats was conducted to assess the distribution (penetration) of E2072 and its homodisulfide dimer in various tissues after single and 5-day daily oral doses (10 mg/kg per day). Blood (by cardiac puncture immediately before sacrifice) and tissues (liver, kidney, brain, and sciatic nerves) were collected at five time points (i.e., 0, 0.5 1, 2, 4, and 8 h after dose). Both E2072 and its homodisulfide were assayed in plasma and tissues by LC-MS/MS.

Bioanalysis of E2072 and Its Homodisulfide. E2072 was stabilized via NEM (Giustarini et al., 2011) in all samples to prevent ex vivo dimerization. E2072 and its homodisulfide were quantified by LC-MS/MS in the biological matrices by the LC-MS/MS method described below.

For quantification of analytes in the plasma samples, the stocks for standards were prepared fresh. Plasma sample (180 μl; or 160 μl of matrix blank and 20 μl of stock for standards), with 10 μl of 100 mM NEM, was allowed to react at room temperature for 30 min followed by the addition of 10 μl of 0.1 N HCl and 20 μl of internal standard, 5 μg/ml in acetonitrile/water (1:1, v/v). The tubes were vortexed, and samples extracted with 400 μl of methanol, followed by vortexing and centrifugation at 10,000 rpm for 5 min. Supernatant (50 μl) was transferred to LC vials, and 5 μl was injected on a LC-MS/MS system. The tissue samples were processed in a manner similar to plasma. In brief, tissue sample was weighed, followed by the addition of phosphate-buffered saline buffer (also containing 10 μl of 100 mM NEM), and volume was adjusted such that all samples were equal per gram tissue. The samples were homogenized, vortexed, and extracted following the same procedure as described for plasma. For each tissue, same matrix was used for the preparation of standard curve. The calibration range was 1 to 5000 ng/ml for both compounds in plasma. For concentrations >5000 ng/ml, samples were diluted with blank matrix before extraction for quantitation. Quality control samples were prepared independently at 50, 250, and 1000 ng/ml for both E2072 and its homodisulfide.

The HPLC system (Agilent Technologies, Santa Clara, CA) coupled with the API 3000 mass spectrometer (Applied Biosystems/MDS Sciex, Toronto, ON, Canada) was used to analyze the extracted samples. Derivatized monomer (E2072) and its dimer were separated on a Luna C18 (2 mm) 30 × 4.60-mm 5 μM column (Phenomenex, Torrance, CA). The mobile phase consisted of acetonitrile (A) and 0.1% formic acid in Milli-Q water (B). Separation was achieved using a gradient run, with the organic composition changing from 50 to 90% over a period of 3 min, maintaining at 90% for 4 min, and then re-equilibrating to 50% over 3 min at a flow rate of 350 μl/min and total run time of 10 min. MS instrument was operated in a negative ion mode. The multiple reaction monitoring (MRM) transition of derivatized E2072 was 426.35 > 301.25 (Q1/Q3); for the E2072-homodisulfide, 601.35 > 266.85; and for the internal standard, 645.25 > 323.25, with a declustering potential of 40 V, entrance potential of 10 V, and collision energy of 21 V for monomer and 40 V for the dimer and internal standard. The curtain gas, ion-spray voltage, temperature, nebulizer gas (GS1), and auxiliary gas (GS2) were set at 8 psi, 5500 V, 350°C, 8 psi, and 4 psi, respectively, and the interface heater was on.

Calibration curves for E2072 and its homodisulfide were constructed from the peak area ratio of the analyte to the internal standard using linear regression, with a weighting factor of 1/(nominal concentration)^2 over the range of 1 to 5000 ng/ml in plasma and tissues. Correlation coefficient >0.99 was obtained in all analytical runs for both analytes. The mean-predicted concentration accuracy ranged from 85.4 to 117% for E2072 and 96.5 to 103% for E2072-homodisulfide standard samples. For quality control samples, the mean-predicted accuracy ranged from 106 to 110% for E2072 and from 95 to 105% for homodisulfide. Both E2072 *N*-ethylmaleimide derivative and its

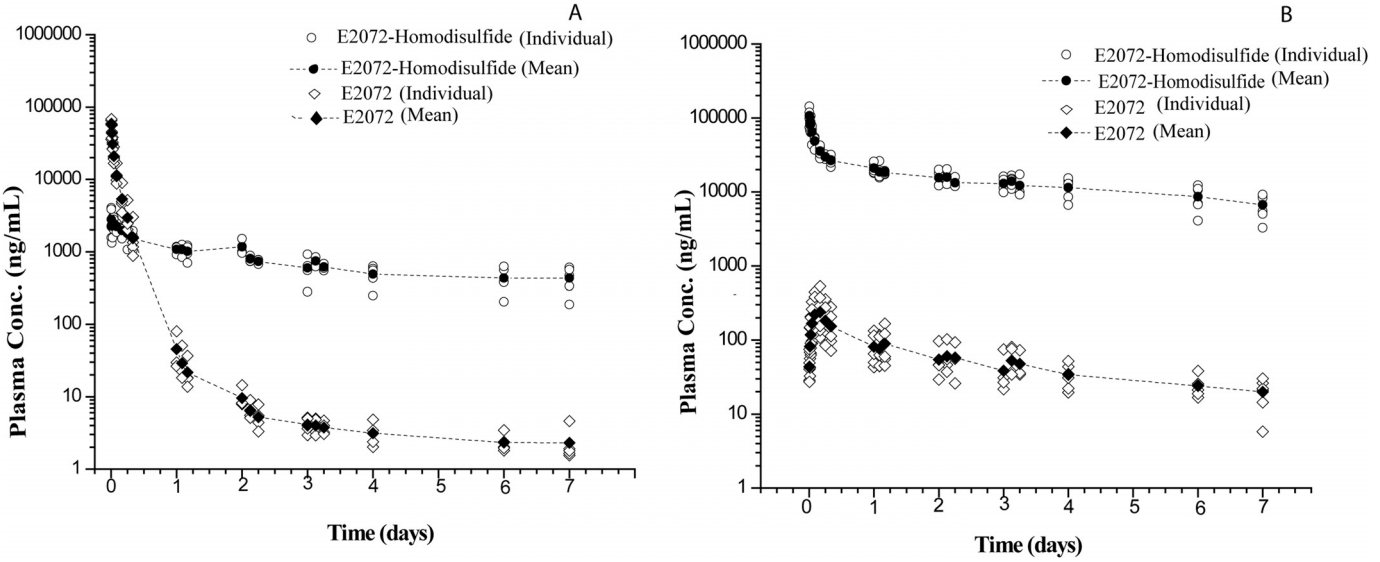

FIG. 4. Plasma concentrations of E2072 and its E0272-homodisulfide in rats after intravenous administration of E2072 at 10 mg/kg (A) and E2072-homodisulfide at 5 mg/kg (B).

TABLE 3

Plasma pharmacokinetic parameters in rats after intravenous administration of E2072 and E2072-homodisulfide[a]

Dose	C_{max}	T_{max}	AUC_{last}	AUC_{inf}	Cl	V_d	$t_{½,\beta}$
	ng/ml	*h*	*ng · h/ml*		*l/h/kg*	*l/kg*	*h*
E2072 (10 mg/kg)							
E2072	57,226 ± 12,077	0.11 ± 0.08	86,652 ± 22,279	86,973 ± 222,349	0.12 ± 0.26	19.0 ± 9.9	105 ± 40
E2072-homodisulfide	3134 ± 838	0.48 ± 0.48	120,303 ± 30,237	253,322 ± 108,052	–	–	208 ± 81
E2072-homodisulfide (5 mg/kg)							
E2072	242 ± 173	3.33 ± 1.03	9149 ± 4386	12,177 ± 5214	–	–	102 ± 27
E2072-homodisulfide	103,952 ± 24,100	0.11 ± 0.08	2,492,590 ± 480,442	3,537,275 ± 1,052,897	0.0015 ± 0.0005	209 ± 52	101 ± 35

[a] Data are presented as mean ± S.D.; n = 5–6 rats per dose group.

homodisulfide were stable in the extracted matrix for at least 24 h on a bench top and in the autosampler.

Pharmacokinetic Analysis of E2072 and Its Homodisulfide. Pharmacokinetic parameters were calculated as implemented in the computer software program WinNonlin version 4.0 (Pharsight, Inc., Mountain View, CA). The maximum plasma concentration (C_{max}) and the time of maximum concentration in plasma (T_{max}) were the observed values. The area under the plasma concentration time curve (AUC) value was calculated to the last quantifiable sample (AUC_{last}) by use of the linear trapezoidal rule. The AUC values were extrapolated to infinity ($AUC_{0-\infty}$) by dividing the last quantifiable concentration (C_t) by the terminal disposition rate constant (λ_z), which was determined from the slope of the terminal phase of the concentration–time profile. Half-life ($t_{½}$) was calculated as 0.693 divided by λ_z. Adjusted R^2 was required to be >0.9, and $\%AUC_{extrap}$ was required to be <25%. Volume of distribution (V_d) was calculated as the dose divided by the product of AUC_∞ and λ_z, and clearance (Cl) was calculated by dividing the dose administered by AUC_∞ (wherever applicable). For intravenous data, Cl and V_d are presented. For oral data, apparent clearance (Cl/F) and apparent volume (V_d/F) are presented. The absolute oral bioavailability, F (%), was calculated using the following equation:

$$F\% = \frac{\text{Mean AUC}_{0-\infty}\text{ (p.o.)}}{\text{Mean AUC}_{0-\infty}\text{ (i.v.)}} \times \frac{\text{Dose (i.v.)}}{\text{Dose (p.o.)}} \times 100$$

Efficacy of E2072 in Rat Chronic Constriction Injury Model. The methods used were as described previously(Bennett and Xie, 1988) using male Sprague- Dawley rats. In brief, the common sciatic nerve was exposed, and four ligatures (4.0 chromic gut) were tied loosely around it with 1-mm spacing. Hyperalgesia testing was initiated 10 days after surgery. Pain sensitivity was assessed by determining withdrawal latencies to a constant thermal stimulus on the plantar surface of the hind paw using a Basile Plantar apparatus (Ugo Basile, Comerio, Italy) according to the method described by Hargreaves et al. (1988). Withdrawal latency, i.e., the time taken for the rat to withdraw its paw from the heat source, was measured to the nearest 0.1 s. The "difference score" was calculated by subtracting the average latency of the nonligated versus ligated side. Statistical analyses were conducted using the Student's t test.

Results

In Vitro Metabolic Stability. Structures of E2072, E2072-homodisulfide, and the internal standard are given in Fig. 1. E2072 was stable in microsomes of mouse, rat, dog, monkey, and human over a period of 1 h as shown in Fig. 2. The lack of substantial disappearance of E2072 during the incubation period (i.e., >90% remaining) indicates stability to phase I oxidation and phase II glucuronidation. In addition, in controls without cofactors, >90% remained at the end of 1 h (data not shown), suggesting compound stability.

In Vitro Blood to Plasma Ratio, Plasma Stability, and Serum Protein Binding. The blood to plasma ratio of E2072 was determined to be 0.68 ± 0.04, indicating preferential partitioning into the extracellular component of blood. The plasma stability was performed in plasma from Sprague-Dawley rats and cynomolgus monkeys. At the end of 1 h, 55 and 64.5% E2072 were extractable in rat plasma at 5 and 10 μM, respectively. In cynomolgus monkey plasma, higher stability was observed, >90% was extractable at the end of 1 h at both concentrations. In addition, the percentage protein binding was high for rat serum (97.5 ± 0.5%) and less in monkey serum (89.9 ± 0.3%). We also evaluated the mass balance of E2072 in blood to plasma ratio, serum protein binding, and plasma stability experiments achieving a recovery of ~100, 70/80 (rat/monkey), and 60/90% (rat/monkey), respectively.

E2072 Pharmacokinetics in Rats. Plasma concentration-time profiles of E2072 in rats after intravenous and oral dosing are shown in Fig. 3. A summary of the plasma pharmacokinetic parameters is listed in Table 1. Absorption of E2072 was relatively rapid after dose. The C_{max} for all doses, i.e., 0.1, 1, 10, and 30 mg/kg, were 62.6 ± 43.0, 1095 ± 1058, 7097 ± 5549, and 13,017 ± 6148 ng/ml, respectively, and were generally observed within 1.5 h after dose. There seemed to be a trend toward delayed T_{max} values with increasing oral doses. The average absolute bioavailability of E2072 was approximately 30% (17–38% range). E2072 plasma concentrations increased with dose after both intravenous and oral administration. $AUC_{0-\infty}$ increased in a less than dose-proportional manner after both intravenous and oral administration, whereas C_{max} was also not dose proportional after oral administration, probably because of the higher variability at lower doses. After the 24-h pharmacokinetic sampling, terminal $t_{1/2}$ mostly ranged from 3 to 4 h.

The effect of food intake on the absorption of E2072 was determined in rats. Table 2 shows E2072 plasma pharmacokinetic param-

TABLE 4

E2072 and E2072-homodisulfide plasma pharmacokinetic parameters in monkeys after intravenous and oral administration of 5 mg/kg E2072[a]

	C_{max}	T_{max}	AUC_{inf}	Cl[b]	V_d[b]	$t_{½,\beta}$	%F
	ng/ml	*h*	*ng · h/ml*	*l/h/kg*	*l/kg*	*h*	
E2072							
i.v.	68,013.3 ± 2698.4	0.08 ± 0.00	63,622.1 ± 7821.8	0.022 ± 0.003	0.72 ± 0.06	23.0 ± 1.2	
p.o.	10,454.3 ± 1032.2	0.42 ± 0.14	24,935.6 ± 740.7	0.057 ± 0.003	0.79 ± 0.31	9.57 ± 3.43	39.1%
E2072-homodisulfide							
i.v.	3272.8 ± 964.8	3.33 ± 1.15	105,771.6 ± 39,413.9	–	–	21.0 ± 0.95	
p.o.	133.6 ± 14.6	5.33 ± 2.31	25,270.8 ± 6198.1	–	–	20.0 ± 1.85	

[a] Data are presented as mean ± S.D.; n = 3 monkeys per dose group.
[b] For intravenous data, Cl and V_d are presented. For oral data, apparent clearance (Cl/F) and apparent volume (V_d/F) are presented.

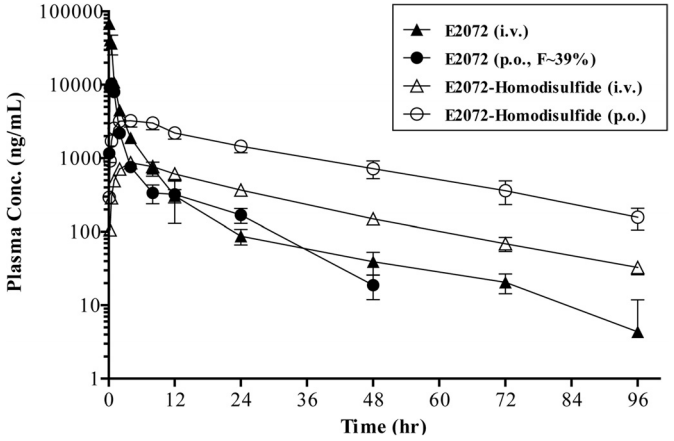

FIG. 5. Plasma concentrations of E2072 and E2072-homodisulfide in cynomolgus monkeys after intravenous bolus and oral administration of E2072 (5 mg/kg).

eters under nonfasted versus fasted conditions. The AUC, clearance, and half-life were comparable under nonfasted and fasted conditions (AUC 37,052 vs. 33,762 ng · h/ml; clearance 0.30 vs. 0.32 l/h/kg; and $t_{½}$ 3.17 vs. 2.75 h, respectively). However, C_{max} values under nonfasted conditions were 2.3 times higher than under fasted conditions (16,186 vs. 7097 ng/ml), respectively.

E2072-Homodisulfide Pharmacokinetics in Rats. Because a common metabolic pathway for sulfhydryl-containing compounds is their interaction with other sulfides to form disulfides, we next investigated E2072's potential to form homodisulfides.

After intravenous administration of 10 mg/kg E2072 (Fig. 4A), both E2072 and its homodisulfide were present in all plasma samples up to 7 days after dose, as shown in Table 3. With the extended pharmacokinetic sampling, E2072 exhibited a biphasic decline in plasma concentration over time with an initial distribution $t_{½,\alpha}$ of 0.87 ± 0.15 h and an unanticipated long elimination $t_{½,\beta}$ of 105 ± 40 h. The homodisulfide of E2072 was observed at the earliest blood sampling time (5 min after dose) and exhibited a terminal $t_{½,\beta}$ of 208 ± 81 h. After intravenous administration of the homodisulfide itself at 5 mg/kg (Fig. 4B), both E2072 and E2072-homodisulfide were present from the earliest blood sampling point (5 min) up to 7 days after dose. E2072-homodisulfide exhibited an initial distribution phase of approximately 6 h in length. C_{max} for E2072 was not observed until 3.3 ± 1.0 h after dose, reflective of an apparent formation phase, probably from the dissociation of the dimer. Both compounds exhibited similar terminal rates of elimination, with $t_{½,\beta}$ values for E2072 and its homodisulfide of 102 ± 27 and 101 ± 35 h, respectively.

It was further validated that observed disulfide concentrations in vivo were not from a contaminant from a dosing solution but rather a metabolite of E2072. This was confirmed by preparing E2072-dosing solution (10 mg/ml) with TCEP at 1.5 mg/ml to prevent the formation of its homodisulfide in the solution. The TCEP-treated dosing solution was administered to rats either intravenously or by oral gavage. Both UV and LC-MS/MS analyses of the solutions confirmed absence of the homodisulfides. Similar pharmacokinetics was observed with TCEP as without TCEP solutions (data not shown).

E2072 and E2072-Homodisulfide Pharmacokinetics in Monkeys. Comparative evaluation of the pharmacokinetic parameters of E2072 and its homodisulfide was performed in male cynomolgus monkeys ($n = 3$) at nominal doses of 5 mg/kg, and blood samples were taken up to 9 days after dose (Table 4). In monkeys, after either intravenous or oral administration (Fig. 5), E2072 exhibited a distribution/elimination phase over approximately the first 24 h, during which the plasma concentrations of E2072 dropped 2 to 3 orders of magnitude. At the end of 24 h, $t_{½}$ for the intravenous profile was 23.0 ± 1.2 h, whereas $t_{½}$ for the oral profile was 9.6 ± 3.4 h. Oral bioavailability for E2072 was approximately 39%. After intravenous dosing, mean V_d was 0.73 l/kg.

After intravenous administration of E2072 (Fig. 5), E2072-homodisulfide was detected in the first 5-min plasma samples. E2072-homodisulfide levels increased over the next few hours until T_{max} was observed at approximately 4 h. Thereafter, homodisulfide declined slowly over the 9 days of the study. Major contrast was observed between the half-lives in monkeys (21.0 ± 0.95 h; Table 4) as opposed to rats where it was approximately 10 times longer (208 ± 81 h; Table 3). Similar to pharmacokinetics of the homodisulfide in rats, the terminal phases for E2072-homodisulfide and E2072 were close to parallel, suggesting that the compounds were related to each other.

After oral administration of E2072 to cynomolgus monkeys (Fig. 5), E2072-homodisulfide was not detected until the 15-min samples. E2072-homodisulfide levels increased over the next few hours until T_{max} was observed at approximately 4 h (Table 4). Thereafter, the

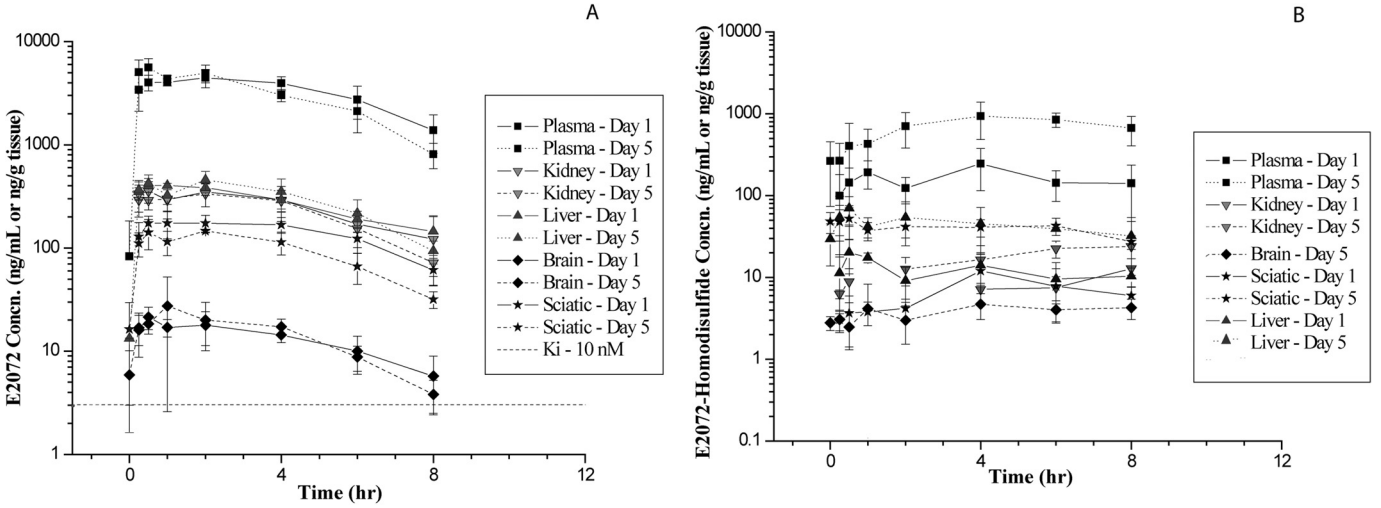

FIG. 6. Concentration-time profiles E2072 (A) and E2072-homodisulfide (B) on days 1 and 5 of oral dosing of 10 mg/kg per day E2072 for 5 consecutive days in male Sprague-Dawley rats.

TABLE 5

E2072 and E2072-homodisulfide rat plasma and tissue concentrations (C_{max}) following 10 mg/kg E2072 administration for 1 or 5 consecutive days[a]

Matrix	E2072 C_{max}[b]		E2072-homodisulfide C_{max}[b]	
	Day 1	Day 5	Day 1	Day 5
Plasma	4922 ± 467	6085 ± 349	240 ± 40	1173 ± 200
Kidney	405 ± 48	388 ± 106	BLQ	23 ± 6
Liver	453 ± 72	457 ± 23	22 ± 10	84 ± 42
Brain	25 ± 3	32.4 ± 21	BLQ	5.5 ± 3.2
Sciatic nerve	203 ± 31	165 ± 30	5.4 ± 1.3	64 ± 15

BLQ, below the limit of quantification.
[a] Data are presented as mean ± S.D.; $n = 4$ rats per dose group.
[b] Plasma (ng/ml) or tissue (ng/g).

homodisulfide declined slowly over the 9 days of the study. Mean $t_{½}$ for E2072-homodisulfide was 20 ± 1.9 h. Because of the limitations of assay sensitivity, the terminal phase of the E2072 profile could not be accurately measured, so it was not apparent whether E2072 assumed a parallel time course with the disulfide after oral administration.

Tissue Distribution after Single and Five Daily Oral Doses. A tissue distribution study in male Sprague-Dawley rats was conducted to assess the distribution of E2072 and its homodisulfide in various tissues after single and 5-day daily oral doses (10 mg/kg per day).

In addition to plasma, E2072 was present in all of the tissues sampled, particularly in sciatic nerve, which is the proposed site of action. Figure 6A illustrates the concentration time profile on days 1 and 5 after single daily oral doses for 5 days. Table 5 lists observed C_{max} values of E2072 in plasma and tissues. The concentrations (C_{max}) in liver and kidney averaged 9.1 and 7.8% of the plasma concentrations, respectively. Concentrations in sciatic nerve, the proposed site of action, averaged 4.2% of plasma concentrations. Apparent brain levels averaged only 0.4% of plasma concentrations, suggesting that E2072 does not achieve appreciable brain penetration. The observed C_{max} values and the concentration-time profiles for E2072 on both days 1 and 5 did not seem to be different in plasma, liver, kidney, or brain tissues upon multiple dosing of E2072, suggesting that little accumulation occurred.

Homodisulfide of E2072 was generally found in all sampled tissues through 8 h after dose (Fig. 6B). The ratios of tissue to plasma concentrations varied, as with E2072, and liver generally exhibited higher levels than kidney or sciatic nerve and very low levels were observed in brain. The observed C_{max} values of E2072-homodisulfide in plasma and the tissues collected were higher on day 5 than on day 1, indicating possible accumulation of the disulfide. The average ratios of E2072-homodisulfide concentrations on day 5 versus day 1 were 4.0 for plasma, 3.9 for liver, and 9.0 for sciatic nerve; ratios for kidney and brain were not calculated because C_{max} could not be determined for these tissues for day 1. Plasma and tissue elimination half-lives and AUCs for disulfide could not be reliably estimated.

The exposure ratios of E2072 to its homodisulfide could not be estimated because of lack of an apparent elimination phase being observed over 24 h for E2072-homodisulfide. However, a measure of the ratio of E2072 to its homodisulfide using C_{max} values showed that, on day 1, the E2072-homodisulfide concentration was 4.9% of the E2072 C_{max} in plasma and 2.7% of the E2072 C_{max} in the sciatic nerve. In contrast, on day 5, the E2072-homodisulfide C_{max} was 19.3% of the E2072 C_{max} in plasma and 38.8% of the E2072 C_{max} in the sciatic nerve.

Efficacy of E2072 in Rat Chronic Constriction Injury Model. Constriction of the sciatic nerve produced thermal hyperalgesia observable at 10 days after surgery on the ligated versus nonligated side. Ten days after hyperalgesia was observed, daily E2072 treatment was initiated. As shown in Table 6, significant reversal of hyperalgesia was seen in rats receiving 10 mg/kg p.o. E2072 daily. It is noteworthy that the analgesic effect continued for at least 7 days after cessation of E2072 treatment. Furthermore, the withdrawal latencies on the nonligated side were similar in E2072 as well as vehicle-treated groups, suggesting that E2072 neither affected normal thermal sensitivity nor impaired the ability to respond to a painful stimulus.

Discussion

The studies conducted here were designed to assess the preclinical pharmacokinetics and metabolism of E2072, a novel, potent, and selective GCP-II inhibitor. In rats, E2072 depicted favorable pharmacokinetic parameters, including consistent oral bioavailability (~30%) and moderate clearance. On the basis of 24-h plasma concentration studies, the $t_{½}$ of E2072 was calculated to be 3 to 4 h. However, longer plasma concentration studies up to 7 days characterized $t_{½,\alpha}$ of 0.87 h and an unanticipated long elimination $t_{½,\beta}$ of approximately 105 h. Food was shown to modestly but selectively increase the C_{max} of E2072. Under nonfasted conditions, the C_{max} of E2072 was 2.3 times higher than under fasted conditions, despite no change in total exposure (AUC), clearance, and volume of distribution. This is different from its thiol analog, 2-MPPA, where concomitant food intake was shown to substantially reduce C_{max} and AUC in clinical studies (van der Post et al., 2005). Tissue distribution studies revealed that E2072 penetrated the sciatic nerve, the proposed target organ in rodents at concentrations almost 10-fold its K_i for GCP-II inhibition up to 8 h after dose. Potential nonlinearity and exposures less than dose proportional were observed after oral administration in rats across the entire range of the administered doses, indicative of either saturable or dose-limiting absorption. The pharmacokinetic parameters in monkeys were similar to those in rats with approximately 39% oral bioavailability and moderate clearance. However, a shorter terminal half-life of approximately 24 h was exhibited in monkeys.

In vivo pharmacokinetic evaluation of E2072 and its homodisulfide was performed in both plasma and tissue in rodents. Examination of the plasma concentration profiles suggests that the E2072-homodisulfide and other possible heterodisulfides were formed rapidly after the intravenous administration of E2072 and that E2072 was reformed as a result of disulfide reduction. Evidence for reversibility of this oxidation-reduction reaction was observed when the E2072-homodisulfide was administered. E2072 did not seem at its maximum plasma

TABLE 6

Thermal hyperalgesia in rats following chronic constriction injury[a,b]

	Following chronic E2072/vehicle daily dosing	4 Days after dose cessation	7 Days after dose cessation	11 Days after dose cessation
E2072 (10 mg/kg per day)	−0.55 ± 0.35*	−1.36 ± 0.11*	−1.53 ± 0.33*	−1.9 ± 0.38
Vehicle	−3.11 ± 0.34	−2.85 ± 0.32	−2.68 ± 0.43	−2.77 ± 0.3

[a] Data are presented as mean ± S.E.M.; *n = 10 rats per dose group.*
[b] Withdrawal latencies to thermal stimulus are presented as the difference score in seconds, calculated by subtracting the average latency on the hind paws nonligated vs. ligated side.
*$P \leq 0.05$ vs. vehicle treated animals.

concentration immediately as might be expected if the monomer was present as a contaminant in the intravenous dosing solution; rather, a phase of increasing concentrations of E2072 was observed after homodisulfide administration, suggesting a period of formation from the disulfide. Furthermore, by 2 to 3 days after administration of either compound, their plasma concentrations followed parallel time courses. It is noteworthy that the sustained exposure of E2072 is consistent with its efficacy in the chronic constrictive injury model of neuropathic pain, where its analgesic effects persisted up to 7 days after dose cessation.

The reactivity of thiol-containing moieties in drugs (captopril, D-penicillamine, SA 96) is a well known phenomenon (Yeung et al., 1983; Yamauchi et al., 1985; Pilkington and Waring, 1988) where the thiol compounds are predominantly metabolized into disulfide metabolites, such as homodisulfides and mixed disulfides (Bourke et al., 1984; Horiuchi et al., 1985). E2072 can exist in three forms in vivo: as free thiol, as homodisulfide, or as a heterodisulfide (bound to either other thiol containing endogenous small molecules or to proteins). It is also possible that E2072's sulfhydryl group could react with its carboxylate to form a thiolactone. However, in an aqueous environment, this formation is unlikely; in a separate study in rats, we found that in vivo administration of the E2072 thiolactone did not readily convert to E2072 (data not shown).

The species difference in half-lives of E2072 (105 h in rats vs. 24 h in monkeys) could be attributed to differences in its interaction with endogenous thiols in plasma to form mixed disulfides. In vitro experiments involving blood to plasma ratio, plasma protein binding, and plasma stability were performed to gain insights into these differences in half-lives. The blood to plasma ratio determinations indicated partitioning primarily into plasma and lower association with red blood cells. The protein binding studies showed higher binding of E2072 to rodent serum (97.5 $\pm$ 0.5%) compared with monkey serum (89.9 $\pm$ 0.3%) proteins. Plasma stability studies indicated that approximately 60% free E2072 remained in rat plasma compared with $>$90% in monkey plasma after a 1-h incubation. The differences between the two species suggest more interactions of E2072 with plasma albumins/proteins probably by formation of reversible protein-thiol-mixed disulfides in rodents compared with primates. Such species differences in plasma albumin reactivity have been described previously (Spiga et al., 2011). It is likely that both the homodisulfide and the mixed disulfides formed in vivo serve as a reversible depot of E2072 and help to maintain the monomer in circulation, which results in its prolonged pharmacological effects. In these short in vitro experiments involving 10- to 60-min incubations, the homodisulfide was found to be $<$4% in both the species, suggesting that the E2072-mixed disulfides may be important in disposition of E2072, although further studies are warranted to substantiate this finding.

Captopril, a marketed angiotensin-converting enzyme inhibitor used primarily as an antihypertensive, demonstrates similar pharmacokinetics where oxidation of the free sulfhydryl group in captopril results in the formation of disulfides conjugates (Yeung et al., 1983; Drummer and Jarrott, 1984; Worland et al., 1984; Drummer et al., 1985). The disulfides of captopril can be reversibly reduced by a combination of enzymatic and redox processes to the monomer. Although this complicates the pharmacokinetics of captopril, this property is thought to contribute to the usefulness of this drug in the clinic, because the disulfides may act as a depot for the monomer and may contribute to its prolonged pharmacological effects.

In summary, the studies presented here report on the pharmacokinetics of E2072 and its homodisulfide. E2072 is a potent, selective, orally available GCP-II inhibitor that has shown promising efficacy in preclinical models of chemotherapy-induced neuropathy and neuropathic pain. Although the pharmacokinetics of E2072 is somewhat complex because of its reversible disulfide formation, resultant prolonged exposures of the parent compound may prove advantageous in providing sustained efficacy results. Currently, additional studies are underway to assess the heterodisulfides formation in vivo following E2072 administration and their effects on the disposition of the parent compound.

Authorship Contributions

Participated in research design: Hoover, Wozniak, Tsukamoto, Rojas, and Slusher.

Conducted experiments: Rais, Hoover, and Alt.

Contributed new reagents or analytic tools: Tsukamoto.

Performed data analysis: Rais, Hoover, and Rudek.

Wrote or contributed to the writing of the manuscript: Rais, Hoover Rudek, Rojas, and Slusher.

References

Akabane T, Tabata K, Kadono K, Sakuda S, Terashita S, and Teramura T (2009) A comparison of pharmacokinetics between humans and monkeys. *Drug Metab Dispos* **38:**308–316.

Bařinka C, Rojas C, Slusher B, and Pomper M (2012) Glutamate carboxypeptidase II in diagnosis and treatment of neurologic disorders and prostate cancer. *Curr Med Chem* **19:**856–870.

Bennett GJ and Xie YK (1988) A peripheral mononeuropathy in rat that produces disorders of pain sensation like those seen in man. *Pain* **33:**87–107.

Bourke CE, Miners JO, and Birkett DJ (1984) Reversible metabolism of D-penicillamine in the rat. *Drug Metab Dispos* **12:**798–799.

Bungay PJ, Tweedy S, Howe DC, Gibson KR, Jones HM, and Mount NM (2011) Preclinical and clinical pharmacokinetics of PF-02413873, a nonsteroidal progesterone receptor antagonist. *Drug Metab Dispos* **39:**1396–1405.

Carozzi VA, Chiorazzi A, Canta A, Lapidus RG, Slusher BS, Wozniak KM, and Cavaletti G (2010) Glutamate carboxypeptidase inhibition reduces the severity of chemotherapy-induced peripheral neurotoxicity in rat. *Neurotox Res* **17:**380–391.

Chen SR, Wozniak KM, Slusher BS, and Pan HL (2002) Effect of 2-(phosphono-methyl)-pentanedioic acid on allodynia and afferent ectopic discharges in a rat model of neuropathic pain. *J Pharmacol Exp Ther* **300:**662–667.

Drummer OH and Jarrott B (1984) Captopril disulfide conjugates may act as prodrugs: disposition of the disulfide dimer of captopril in the rat. *Biochem Pharmacol* **33:**3567–3571.

Drummer OH, Thompson J, Hooper R, and Jarrott B (1985) Effect of probenecid on the disposition of captopril and captopril dimer in the rat. *Biochem Pharmacol* **34:**3347–3351.

Fukuda H, Ohashi R, Tsuda-Tsukimoto M, and Tamai I (2008) Effect of plasma protein binding on in vitro-in vivo correlation of biliary excretion of drugs evaluated by sandwich-cultured rat hepatocytes. *Drug Metab Dispos* **36:**1275–1282.

Ghadge GD, Slusher BS, Bodner A, Canto MD, Wozniak K, Thomas AG, Rojas C, Tsukamoto T, Majer P, Miller RJ, et al. (2003) Glutamate carboxypeptidase II inhibition protects motor neurons from death in familial amyotrophic lateral sclerosis models. *Proc Natl Acad Sci USA* **100:**9554–9559.

Giustarini D, Dalle-Donne I, Milzani A, and Rossi R (2011) Detection of glutathione in whole blood after stabilization with N-ethylmaleimide. *Anal Biochem* **415:**81–83.

Harada C, Harada T, Slusher BS, Yoshida K, Matsuda H, and Wada K (2000) N-acetylated-alpha-linked-acidic dipeptidase inhibitor has a neuroprotective effect on mouse retinal ganglion cells after pressure-induced ischemia. *Neurosci Lett* **292:**134–136.

Hargreaves K, Dubner R, Brown F, Flores C, and Joris J (1988) A new and sensitive method for measuring thermal nociception in cutaneous hyperalgesia. *Pain* **32:**77–88.

Horiuchi M, Takashina H, Iwatani T, and Iso T (1985) [Study on metabolism of the dithiol compound. I. Isolation and identification of metabolites of N-(2-mercapto-2-methylpropanoyl)-L- cysteine (SA96) in the blood and urine of the rat]. *Yakugaku Zasshi* **105:**665–670.

Jackson PF, Tays KL, Maclin KM, Ko YS, Li W, Vitharana D, Tsukamoto T, Stoermer D, Lu XC, Wozniak K, et al. (2001) Design and pharmacological activity of phosphinic acid based NAALADase inhibitors. *J Med Chem* **44:**4170–4175.

Jayaraman R, Pilla Reddy V, Pasha MK, Wang H, Sangthongpitag K, Yeo P, Hu CY, Wu X, Xin L, Goh E, et al. (2011) Preclinical metabolism and disposition of SB939 (Pracinostat), an orally active histone deacetylase inhibitor, and prediction of human pharmacokinetics. *Drug Metab Dispos* **39:**2219–2232.

Luszczki JJ, Mohamed M, and Czuczwar SJ (2006) 2-phosphonomethyl-pentanedioic acid (glutamate carboxypeptidase II inhibitor) increases threshold for electroconvulsions and enhances the antiseizure action of valproate against maximal electroshock-induced seizures in mice. *Eur J Pharmacol* **531:**66–73.

Majer P, Jackson PF, Delahanty G, Grella BS, Ko YS, Li W, Liu Q, Maclin KM, Poláková J, Shaffer KA, et al. (2003) Synthesis and biological evaluation of thiol-based inhibitors of glutamate carboxypeptidase II: discovery of an orally active GCP II inhibitor. *J Med Chem* **46:**1989–1996.

Marmiroli P, Slusher B, and Cavaletti G (2012) Tissue distribution of glutamate carboxypeptidase II (GCPII) with a focus on the central and peripheral nervous system. *Curr Med Chem* **19:**1277–1281.

Neale JH, Olszewski RT, Gehl LM, Wroblewska B, and Bzdega T (2005) The neurotransmitter *N*-acetylaspartylglutamate in models of pain, ALS, diabetic neuropathy, CNS injury and schizophrenia. *Trends Pharmacol Sci* **26:**477–484.

Neale JH, Olszewski RT, Zuo D, Janczura KJ, Profaci CP, Lavin KM, Madore JC, and Bzdega T (2011) Advances in understanding the peptide neurotransmitter NAAG and appearance of a new member of the NAAG neuropeptide family. *J Neurochem* **118:**490–498.

Pilkington AE and Waring RH (1988) The metabolism and disposition of D-penicillamine in the DA-strain rat. *Eur J Drug Metab Pharmacokinet* **13:**99–104.

Rahn KA, Slusher BS, and Kaplin AI (2012) Glutamate in CNS neurodegeneration and cognition and its regulation by GCPII inhibition. *Curr Med Chem* **19:**1335–1345.

Slusher BS, Robinson MB, Tsai G, Simmons ML, Richards SS, and Coyle JT (1990) Rat brain N-acetylated alpha-linked acidic dipeptidase activity. Purification and immunologic characterization. *J Biol Chem* **265:**21297–21301.

Slusher BS, Vornov JJ, Thomas AG, Hurn PD, Harukuni I, Bhardwaj A, Traystman RJ, Robinson MB, Britton P, Lu XC, et al. (1999) Selective inhibition of NAALADase, which converts NAAG to glutamate, reduces ischemic brain injury. *Nat Med* **5:**1396–1402.

Spiga O, Summa D, Cirri S, Bernini A, Venditti V, De Chiara M, Priora R, Frosali S, Margaritis A, Di Giuseppe D, et al. (2011) A structurally driven analysis of thiol reactivity in mammalian albumins. *Biopolymers* **95:**278–285.

Stoermer D, Vitharana D, Hin N, Delahanty G, Duvall B, Ferraris DV, Grella BS, Hoover R, Rojas C, Shanholtz MK, et al. (2012) Design, synthesis, and pharmacological evaluation of glutamate carboxypeptidase II (GCPII) inhibitors based on thioalkylbenzoic acid scaffolds. *J Med Chem* **55:**5922–5932.

Tsukamoto T, Flanary JM, Rojas C, Slusher BS, Valiaeva N, and Coward JK (2002) Phosphonate and phosphinate analogues of N-acylated gamma-glutamylglutamate. potent inhibitors of glutamate carboxypeptidase II. *Bioorg Med Chem Lett* **12:**2189–2192.

van der Post JP, de Visser SJ, de Kam ML, Woelfler M, Hilt DC, Vornov J, Burak ES, Bortey E, Slusher BS, Limsakun T, et al. (2005) The central nervous system effects, pharmacokinetics and safety of the NAALADase-inhibitor GPI 5693. *Br J Clin Pharmacol* **60:**128–136.

Witkin JM, Gasior M, Schad C, Zapata A, Shippenberg T, Hartman T, and Slusher BS (2002) NAALADase (GCP II) inhibition prevents cocaine-kindled seizures. *Neuropharmacology* **43:**348–356.

Worland PJ, Drummer OH, and Jarrott B (1984) Gastric and intestinal absorption of captopril in acutely and chronically treated rats: comparison with salicylic acid. *J Pharm Sci* **73:**1755–1758.

Wozniak KM, Rojas C, Wu Y, and Slusher BS (2012) The role of glutamate signaling in pain processes and its regulation by GCP II inhibition. *Curr Med Chem* **19:**1323–1334.

Xi ZX, Kiyatkin M, Li X, Peng XQ, Wiggins A, Spiller K, Li J, and Gardner EL (2010a) N-Acetylaspartylglutamate (NAAG) inhibits intravenous cocaine self-administration and cocaine-enhanced brain-stimulation reward in rats. *Neuropharmacology* **58:**304–313.

Xi ZX, Li X, Peng XQ, Li J, Chun L, Gardner EL, Thomas AG, Slusher BS, and Ashby CR Jr (2010b) Inhibition of NAALADase by 2-PMPA attenuates cocaine-induced relapse in rats: a NAAG-mGluR2/3-mediated mechanism. *J Neurochem* **112:**564–576.

Yamamoto T, Nozaki-Taguchi N, and Sakashita Y (2001a) Spinal N-acetyl-alpha-linked acidic dipeptidase (NAALADase) inhibition attenuates mechanical allodynia induced by paw carrageenan injection in the rat. *Brain Res* **909:**138–144.

Yamamoto T, Nozaki-Taguchi N, Sakashita Y, and Inagaki T (2001b) Inhibition of spinal N-acetylated-alpha-linked acidic dipeptidase produces an antinociceptive effect in the rat formalin test. *Neuroscience* **102:**473–479.

Yamauchi H, Morikawa K, Kuwano M, Hikida M, Fujimura K, Horiuchi M, Uemura O, and Iso T (1985) [Pharmacological studies of N-(2-mercapto-2-methylpropionyl)-L- cysteine (SA 96). VI. Effects on vitamin B6, metals and skin collagen in rats]. *Nihon Yakurigaku Zasshi* **86:**25–33.

Yeung JH, Breckenridge AM, and Park BK (1983) Drug protein conjugates–VI. Role of glutathione in the metabolism of captopril and captopril plasma protein conjugates. *Biochem Pharmacol* **32:**3619–3625.

Zhang W, Murakawa Y, Wozniak KM, Slusher B, and Sima AA (2006) The preventive and therapeutic effects of GCPII (NAALADase) inhibition on painful and sensory diabetic neuropathy. *J Neurol Sci* **247:**217–223.

Zhang W, Slusher B, Murakawa Y, Wozniak KM, Tsukamoto T, Jackson PF, and Sima AA (2002) GCPII (NAALADase) inhibition prevents long-term diabetic neuropathy in type 1 diabetic BB/Wor rats. *J Neurol Sci* **194:**21–28.

Address correspondence to: Dr. Barbara S. Slusher, Johns Hopkins Brain Science Institute, NeuroTranslational Drug Discovery Program, 855 North Wolfe St., Baltimore, MD 21205. E-mail: bslusher@jhmi.edu